Evaluation of 1-Site and 5-Site Models of Methane on Its Adsorption on Graphite and in Graphitic Slit Pores

D. D. Do* and H. D. Do

Department of Chemical Engineering, University of Queensland, St. Lucia, Qld 4072, Australia

Received: May 11, 2005; In Final Form: August 25, 2005

In this paper, we evaluate the performance of the 1- and 5-site models of methane on the description of adsorption on graphite surfaces and in graphitic slit pores. These models have been known to perform well in the description of the fluid-phase behavior and vapor−liquid equilibria. Their performance in adsorption is evaluated in this work for nonporous graphitized thermal carbon black, and simulation results are compared with the experimental data of Avgul and Kiselev (*Chemistry and Physics of Carbon*; Dekker: New York, 1970; Vol. 6, p 1). On this nonporous surface, it is found that these models perform as well on isotherms at various temperatures as they do on the experimental isosteric heat for adsorption on a graphite surface. They are then tested for their performance in predicting the adsorption isotherms in graphitic slit pores, in which we would like to explore the effect of confinement on the molecule packing. Pore widths of 10 and 20 Å are chosen in this investigation, and we also study the effects of temperature by choosing 90.7, 113, and 273 K. The first two are for subcritical conditions, with 90.7 K being the triple point of methane and 113 K being its boiling point. The last temperature is chosen to represent the supercritical condition so that we can investigate the performance of these models at extremely high pressures. We have found that for the case of slit pores investigated in this paper, although the two models yield comparable pore densities (provided the accessible pore width is used in the calculation of pore density), the number of particles predicted by the 1-site model is always greater than that predicted by the 5-site model, regardless of whether temperature is subcritical or supercritical. This is due to the packing effect in the confined space such that a methane molecule modeled as a spherical particle in the 1-site model would pack better than the fused five-sphere model in the case of the 5-site model. Because the 5-site model better describes the liquid- and solid-phase behavior, we would argue that the packing density in small pores is better described with a more detailed 5-site model, and care should be exercised when using the 1-site model to study adsorption in small pores.

1. Introduction

Adsorption of gases on nonporous surfaces and in porous solids has been increasingly understood, and this is credited to the now-established molecular simulation methods such as Monte Carlo (MC), molecular dynamics[2,3] (MD), and density functional theory[4−6] (DFT). Equilibria of simple gases are now routinely studied with these tools, and the predicted adsorption equilibria in the form of isotherm generally agree well with experimental data, at least on nonporous graphitized thermal carbon black, for which reliable and accurate experimental data are available in the literature.[1,7,8] However, the success of the predictions from any of these molecular simulation tools depends on the choice of the potential equations and mostly on the selection of the molecular parameters. For simple gases such as noble gases and methane, the simple 12−6 LJ equation is quite adequate, especially for noble gases, as they are spherical atoms. For the case of methane, however, it is modeled as a pseudo-spherical particle with one interaction center. It is also modeled as a 5-site model by a number of authors. The 5-site model has mostly been used to study the liquid and solid behavior, and its use in adsorption has not been investigated. Because methane is one of the high-energy gases, and its potential utilization by storage in porous materials at high pressure (but still lower than the pressure used in CNG) is an alternative to gasoline, it is important to evaluate the various models of methane in adsorption to see whether the 1-site model is as good as the 5-site model, which is known to yield better liquid and solid behavior of the homogeneous fluid.[9,10] If that is the case, then the 1-site model should be a preferred choice, as it is substantially cheaper to use than the 5-site model for predicting methane adsorption capacity and isosteric heat in adsorption study and design, and using the 5-site model is extremely expensive in terms of computation time. Our investigation will cover a range of temperatures to study the effect of subcritical and supercritical conditions, and a range of pressures to study the compression effect. Different pore sizes are also studied, to investigate the effect of strength of the solid−fluid potential.

2. Theory

Although there are many models that have been proposed for methane in the literature, we chose the 1-site model suggested by Martin and Siepmann,[11] and the 5-site model, in which five atoms in the methane molecule are explicitly accounted for, of Kollman and co-workers[12] in this investigation. Our objective is to determine whether the simpler 1-site model is suitable for describing adsorption on a graphitized thermal

* To whom all correspondence should be addressed. Ph: +61-7-3365-4154. Fax: +61-7-3365-2789. E-mail: duongd@cheque.uq.edu.au.

10.1021/jp052448y CCC: $30.25
Published on Web 09/27/2005

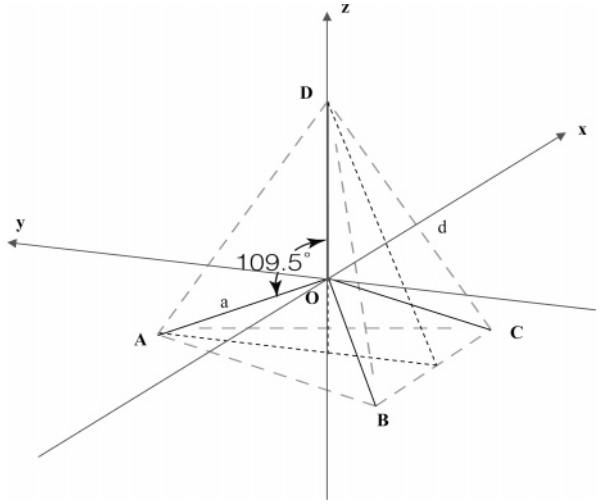

Figure 1. Molecular frame of the coordinates of methane.

carbon black (GTCB) surface and in slit pores of various sizes, ranging from small pores to nanopores. Temperature effects will also be investigated. The potential energy of interaction is assumed to follow the LJ equation

$$\varphi_{i,j}^{(a,b)} = 4\epsilon^{(a,b)}\left[\left(\frac{\sigma^{(a,b)}}{r_{i,j}^{(a,b)}}\right)^{12} - \left(\frac{\sigma^{(a,b)}}{r_{i,j}^{(a,b)}}\right)^{6}\right] \tag{1a}$$

which describes the potential energy between site *a* on particle *i* and site *b* on particle *j*. We use subscripts to denote particles and superscripts for sites, and the order of sites in the superscript matches the order of particles in the subscript. For example, in the above equation, we have site *a* of particle *i* and site *b* of particle *j*. If the site−site interaction is known, the potential energy of interaction between two particles is simply

$$\varphi_{i,j} = \sum_{a=1}^{M}\sum_{b=1}^{M}\varphi_{i,j}^{(a,b)} \tag{1b}$$

where M is the number of sites in the model. For the 1-site model, $M = 1$, whereas for the 5-site model, $M = 5$. The molecular parameters for the 1-site model are taken from Martin and Siepmann,[11] whereas those for the 5-site models are from Sun et al.[12] The parameters for the Martin and Siepmann 1-site model are $\sigma = 3.73$ Å and $\epsilon/k_B = 148$ K. For the Kollman 5-site model,[12] methane is modeled as a 5-dispersive-interaction-site model, with one site positioned at the center of the carbon atom, and the other four sites located at the centers of four hydrogen atoms. The octopole moment of methane is also accounted for in the Kollman model.[12] They assigned a positive partial charge of 0.165 e to each hydrogen atom and a negative partial charge of −0.66 e to the carbon atom. They used the carbon−hydrogen bond length of 1.09 Å, and the angle H−C−H is 109.5°. To account for the orientation of the methane molecule of the 5-site model in the Monte Carlo simulation, we assign each molecule its own molecular frame coordinate. It is chosen such that the origin is at the center of the carbon atom, as shown in Figure 1. The molecular *x*-axis is chosen such that is passes through the origin and is parallel to one of the vectors pointing from one hydrogen atom to another hydrogen atom (BC in Figure 1). The *z*-axis passes through the origin and one of the hydrogen atoms as shown as OD in Figure 1, and the *y*-axis is as shown. In the Monte Carlo simulation, one of the moves is a rotation, and the rotation of the methane molecule is effected in the simulation by rotating a randomly selected particle around each of the three molecular axes of equal probability.

TABLE 1: Molecular Coordinates of the Five Sites of Methane

site	*x*	*y*	*z*
carbon	0	0	0
hydrogen 1	0	$d\sqrt{3}/3$[a]	$-a/3$[b]
hydrogen 2	$-d/2$	$-d\sqrt{3}/6$	$-a/3$
hydrogen 3	$d/2$	$-d\sqrt{3}/6$	$-a/3$
hydrogen 4	0	0	a

[a] Where d is the distance joining two sites (other than the carbon site), and is given by $d^2 = 2a^2(1 - \cos\theta)$, with θ being 109.5°. [b] For the Kollman model, the parameter a is the carbon−hydrogen bond length, which was taken to be 1.09 Å.

Let the distance between the carbon atom center and one of the other four sites be *a*. This is the C−H bond length in the model by Kollman and co-workers[12] ($a = 1.09$ Å). With respect to the molecular frame coordinate shown in Figure 1, the coordinates of the carbon site and the four other sites are given in Table 1 below.

The 5-site model for methane by Kollman and co-workers[12] has the following parameters. The molecular parameters of the carbon atom are $\sigma = 3.4$ Å and $\epsilon/k = 55.055$ K, and those of the hydrogen atom are $\sigma = 2.65$ Å and $\epsilon/k = 7.901$ K. This model has the collision diameter for carbon atom at 3.4 Å, which is consistent with other values reported in the literature for the carbon atom. The well depth of the carbon atom in methane is 55 K, compared to a value of 28 K for the carbon atom in a graphite layer. The difference is that the carbon atom of methane has sp^3 hybridization, whereas the carbon atom in the graphite layer has sp^2 hybridization.

We have just addressed the interaction energy between two methane molecules in which the interaction is due to a dispersive force. In the 5-site model by Kollman, a set of discrete charges is assigned to each methane molecule. The interaction between a charge on one molecule and a charge on another molecule can be carried out exactly the same way as done with the dispersive interaction sites above. The interaction energy due to electrostatic force between a charge α on a molecule *i* and a charge β on a molecule *j* is determined via the Coulomb law of electrostatic interaction

$$\varphi_{q;i,j}^{(\alpha,\beta)} = \frac{1}{4\pi\epsilon_0}\frac{q_i^{\alpha}\, q_j^{\beta}}{r_{i,j}^{(\alpha,\beta)}} \tag{2}$$

where ϵ_0 is the permittivity of free space ($\epsilon_0 = 10^7/(4\pi c^2) = 8.8543 \times 10^{-12}$ C^2 J^{-1} m^{-1}; c is the speed of light), $r_{i,j}^{(\alpha,\beta)}$ is the distance between two charges α and β on molecules *i* and *j*, respectively, q_i^{α} is the value of charge α on molecule *i*, and q_j^{β} is the value of charge β on molecule *j*. The electrostatic interaction between two molecules takes the form $\varphi_{q;i,j} = \sum_{\alpha=1}^{M_q}\sum_{\beta=1}^{M_q}\varphi_{q;i,j}^{(\alpha,\beta)}$. Here, M_q is the number of charges on the molecule ($M_q = 5$).

The solid−fluid potential between a site and the surface is assumed to take the form of the Steele 10-4-3 equation.[13] For the 5-site model, each of the five sites interacts with the graphite surface following the same equation. The solid−fluid well depth of interaction energy is calculated with the following equation

$$\epsilon^{(\text{methane,carbon})} = (1 - k)\sqrt{\epsilon^{(\text{methane,methane})} \times \epsilon^{(\text{carbon,carbon})}}$$

where *k* is the binary interaction parameter, and we assume that

this binary interaction parameter is the same for all five interaction sites in the 5-site models. The well depth for the carbon atom in the graphite is 28 K. The Steele 10-4-3 equation describes the interaction between a fluid particle *i* and a lattice with its sublattices, and it is given by

$$\varphi^{(a,b)}_{i,\text{lattice with sublattices}} = \varphi_w\left[\frac{1}{5}\left(\frac{\sigma^{(a,b)}}{z}\right)^{10} - \frac{1}{2}\left(\frac{\sigma^{(a,b)}}{z}\right)^{4} - \frac{(\sigma^{(a,b)})^4}{6\Delta(z+0.61\Delta)^3}\right] \quad (3a)$$

where *a* and *b* denote methane and carbon, respectively. Here, the wall potential energy parameter φ_w is given by

$$\varphi_w = 4\pi\rho_s\epsilon^{(a,b)}[\sigma^{(a,b)}]^2 \quad (3b)$$

where ρ_s is the density of carbon atoms per unit surface area of the graphite layer, which is taken to be composed of condensed benzene rings with a carbon−carbon bond length of 1.42 Å (ρ_s = 0.382 Å^{-2}). The collision diameter of a carbon atom in the graphite layer is 3.4 Å.

Grand Canonical Monte Carlo Simulation. The molecular simulation method employed in this paper is the grand canonical Monte Carlo (GCMC) simulation. The parameters associated with the MC simulation used in this paper are the following: (i) the box length in the case of the slit pore is at least 10 times the collision diameter, (ii) the cutoff radius is taken to be half of the box length, (iii) the number of cycles for the equilibration step is 50 000, and that for the statistics collection is also 50 000, and (iv) in each cycle, there are *N* displacement moves and *N* rotations (in the case of 5-site model) where *N* is the number of particles in the simulation box.

The GCMC method not only gives information about the average number of particles in the box but also yields information about the isosteric heat. This isosteric heat has two contributions, which are not mutually exclusive. One is the solid−fluid interaction,and the other is the fluid−fluid interaction. We describe briefly below the necessary equations for the computation of isosteric heats. It is defined as the difference between the molar enthalpy of adsorbate in the vapor phase and the partial molar enthalpy of the adsorbed phase[14] ($\bar{h}_a = (\partial H_a/\partial N_a)_{P,T}$.

$$-\Delta h = h_G - \bar{h}_a \quad (4)$$

The molar enthalpy is the sum of the molar internal energy and the product of the pressure and molar volume of that phase. With the approximation of ideal gas behavior for the gas phase and negligible molar volume for the adsorbed phase, we approximated the above equation by $-\Delta h = R_g T + e_G - \bar{e}_a$, where *e* is the molar internal energy. If the kinetic energy does not change upon adsorption, the difference in the internal energy is equal to the difference in the potential energy. Therefore, eq 4 is approximated by $-\Delta h = R_g T + u_G - \bar{u}_a$. The partial molar potential energy is calculated by applying the fluctuation theory,[15,16] and it can be expressed as the ensemble average of the potential energy, number of particles, and their products as follows[17]

$$-\Delta h = R_g T - \frac{\langle U_{a,ext}N\rangle - \langle U_{a,ext}\rangle\langle N\rangle}{\langle N^2\rangle - \langle N\rangle^2} \quad (5)$$

where $U_{a,ext}$ is the potential energy between adsorbate molecules plus that between adsorbate molecule and the solid substrate. The potential energy of the interaction can be broken down into contributions of fluid−fluid interaction and fluid−solid interaction

$$-\Delta h = \left[R_g T - \frac{\langle U_{a,ff}N\rangle - \langle U_{a,ff}\rangle\langle N\rangle}{\langle N^2\rangle - \langle N\rangle^2}\right] - \frac{\langle U_{a,sf}N\rangle - \langle U_{a,sf}\rangle\langle N\rangle}{\langle N^2\rangle - \langle N\rangle^2} \quad (6)$$

The square bracket term in the above equation is the contribution of fluid−fluid interaction to the isosteric heat of adsorption, whereas the last term is the contribution from the fluid−solid interaction.

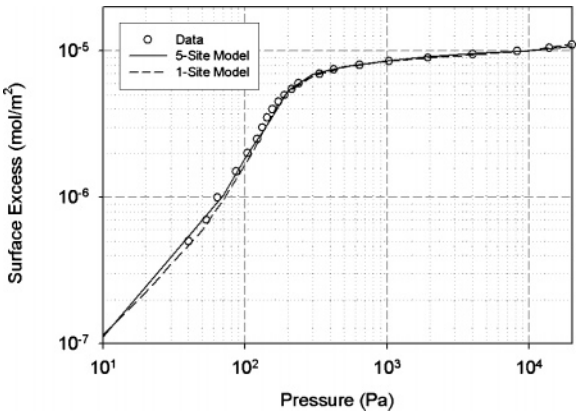

Figure 2. Adsorption isotherm of methane on graphitized thermal carbon black at 113 K (experimental data from Avgul and Kiselev,[1] circle symbols; 5-site model, solid line; 1-site model, dashed line).

3. Results and Discussion

3.1. Graphitized Thermal Carbon Black. To compare the performance of the 1- and 5-site models, we used the experimental data of methane for adsorption capacity and isosteric heat on graphitized thermal carbon black from Avgul and Kiselev.[1] Isotherms at 113, 123, 133, and 143 K were reported by these authors. These data are very accurate and reliable, and therefore they are suitable for testing the models' capabilities for predicting adsorption isotherms. We first used the isotherm at 113 K to compare the performance of these models. The results are shown in Figure 2, where we plot the surface excess (mol/m^2) versus pressure (Pa) in a log−log plot. The experimental data are presented as circle symbols, whereas the results from the 1-site model are shown as the dashed line and those from the Kollman 5-site model as the solid line.

These models describe extremely well the Henry law constant, and this is the case because we adjust the solid−fluid well depth of interaction energy with the binary interaction parameter (*k*) to match the experimental Henry constant. These binary interaction parameters for the 1-site and 5-site models are −0.02 and −0.07, respectively. On observation of the isotherm shown in Figure 2, we see practically no difference between these models, at least within the experimental and simulation errors.

Having seen the comparable performance of these models on the description of the adsorption isotherm at 113 K on graphitized thermal carbon black, we now test their performance on the description of the isosteric heat with respect to loading. The GCMC simulated isosteric heat is shown in Figure 3 for these models as a function of loading. Within the experimental and simulation errors, we again cannot draw any distinction, suggesting that both models describe reasonably well the isosteric heat of adsorption of methane on an open surface.

Having done the evaluation of the 1- and 5-site models on their performance against the adsorption isotherm and isosteric heat at 113 K, we further evaluate them with the 123, 133, and

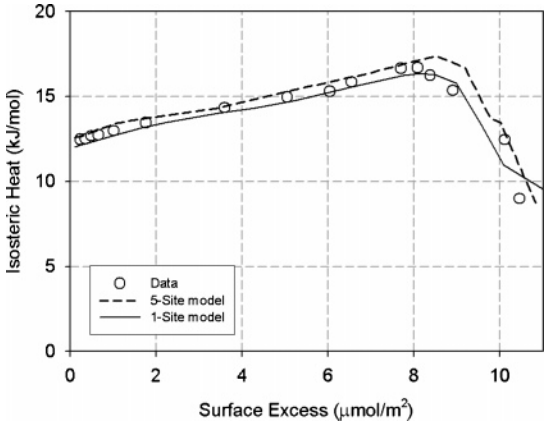

Figure 3. Isosteric heat versus loading (symbols, experimental data; solid line, 1-site model; dashed line, 5-site model).

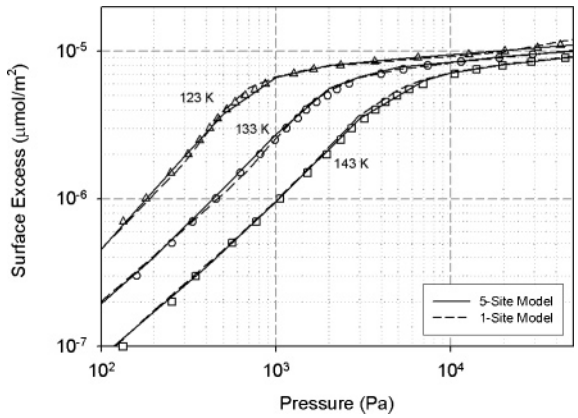

Figure 4. Adsorption isotherms of methane on graphitized thermal carbon black at 123 (top curve), 133 (middle curve), and 143 K (bottom curve) (solid lines: 5-site model; dashed line: 1-site model; symbols: experimental data of Avgul and Kiselev[1]).

143 K data of adsorption on graphitized thermal carbon black. The results are shown in Figure 4. We see that the performance of these models is again quite comparable, and they correctly describe the experimental Henry constants, 0.0143, 0.005, 0.002, and 0.000857 μmol Pa^{-1} m^{-2} at 113, 123, 133, and 143 K, respectively. The Claperon equation is applied to these values of the Henry constant, and we obtain a heat of adsorption at zero loadings of 12.6 kJ/mol, which is in perfect agreement with the GCMC simulation results, as shown in Figure 3.

Thus from the standpoint of describing the adsorption of methane on an open surface for engineering purposes, the 1-site model is regarded to be as good as the 5-site model, and it is substantially cheaper to compute.

Having described the adsorption behavior on nonporous graphitized thermal carbon black, where molecules experience no constraint in volume space for adsorption (i.e., no packing effect), we would like to investigate the performance of these models for the description of methane adsorption in the confined space of slit pores. To fully evaluate this, we study pores of different sizes and adsorption conditions.

3.2. Slit Pores. Let us now turn to the investigation of the adsorption in the confined space of micropores and nanopores (slit shape) under subcritical and supercritical conditions, to investigate the confinement effect. The conditions listed in Table 2 will be explored in the simulation.

For the upper end of the pressure range in the case of 113 K and the pressure range at 273 K, methane does not behave as an ideal gas, and separate simulations need to be conducted in the bulk phase to relate pressure and the chemical potential (activity), which is then used in the GCMC of slit pores to determine the adsorption isotherm and isosteric heat.

TABLE 2: Conditions Used in the GCMC Simulation of Three Models in Graphitic Slit Pores

pore width (Å)	temperature (K)	conditions	vapor pressure (Pa)	
10	90.7	subcritical	11 700	triple point
	113	subcritical	113 200	boiling point
	273	supercritical		
20	113	subcritical	113 200	boiling point

TABLE 3: Pressure and Liquid Densities of Methane at Various Points

	T (K)	pressure (Pa)	liquid density (kmol/m^3)
triple point	90.7	11 700	28.216
boiling point	113	113 200	26.273
critical point	190.6	4 600 000	10.101

The properties of methane at the triple point, boiling point, and critical point are given in Table 3. These values of density are used later to compare with the pore density, which depends critically on the definition of the pore volume accessible to adsorbate molecules.

Accessible Pore Volume and Width. The accessible pore volume could be defined in a way such that the center of the molecule should be available in the volume space where the solid−fluid potential is negative. So if we let z_0 be the distance at which the solid−fluid potential is zero, the volume space available to the fluid molecule is

$$V = (H - 2z_0 + \sigma_{ff})\ \text{Å} \tag{7}$$

(Figure 5 shows the typical solid−fluid potential in a slit pore). Here, H is the physical width of the pore, which is defined as the distance from the plane passing through all carbon atoms of the outermost layer of one wall to the corresponding plane of the opposite wall. So we will take the accessible width for adsorbate molecule as $H' = H - 2z_0 + \sigma_{ff}$ in this work. This formula was first suggested by Everett and Powl,[18] and later by Kaneko et al.[19]

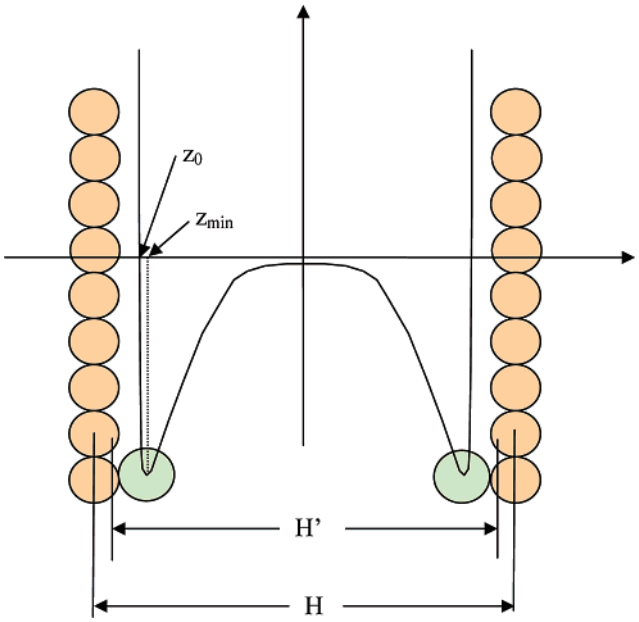

Figure 5. Definition of the accessible pore width H' and the physical pore width H.

TABLE 4: Relationship between Zero-Potential Distance z_0 and Physical Width H

H (Å)	$z_0/\sigma^{(CH_4,C)}$	H (Å)	$z_0/\sigma^{(CH_4,C)}$	H (Å)	$z_0/\sigma^{(CH_4,C)}$	H (Å)	$z_0/\sigma^{(CH_4,C)}$	H (Å)	$z_0/\sigma^{(CH_4,C)}$
6.5	0.81523	9.5	0.84221	12.5	0.84752	15.5	0.84874	18.5	0.84915
7	0.82068	10	0.84382	13	0.84784	16	0.84884	19	0.84919
7.5	0.82739	10.5	0.84501	13.5	0.84810	16.5	0.84893	20	0.84926
8	0.83289	11	0.84590	14	0.84831	17	0.84900	30	0.84948
8.5	0.83701	11.5	0.84658	14.5	0.84848	17.5	0.84906	50	0.84954
9	0.84002	12	0.84711	15	0.84863	18	0.84911	100	0.84955

Obviously the distance z_0 would depend on the pore width; however, this dependence is very weak for large pores, and for such cases we can take z_0 as the value associated with that corresponding to a single surface ($z_0/\sigma^{(CH_4,C)} = 0.84955$). For the case of the 1-site model of methane, $\sigma^{(CH_4,C)} = 3.565$ Å (calculated with the Lorentz−Berthelot mixing rule), and we find from the use of the Steele 10-4-3 equation that $z_0 = 3.0286$ Å. Thus the accessible width is then

$$H' = H - 2z_0 + \sigma_{ff} = H - 2.327 \tag{8}$$

where the unit for width is Å. For small pores, the parameter z_0 is a function of H, and it is given in Table 4, where we see that for pore widths greater than about 20 Å, the value for z_0 does not change very much with the pore width, and it can be taken as the value corresponding to a single wall ($z_0 = 3.0286$ Å). However, when the width is less than 20 Å, z_0 changes with H, and should be accounted for properly.

We have discussed the accessible volume for the 1-site model. For the 5-site models, the accessible volume will depend on the orientation of the methane molecule. We consider two specific orientations. One is the pyramid configuration with its base parallel and close to the graphite surface. The other is the inverted pyramid configuration. Figure 6 shows the solid−fluid potential versus distance from the plane passing through all the carbon atoms of the outermost layer to the closest site on the methane molecule. We see that the pyramid configuration has a deeper minimum but it is further from the graphite surface (larger z_0) than the inverted pyramid configuration. The distance z_0 is the distance at which the solid−fluid potential is zero, and we will take the value of the pyramid configuration to determine the accessible width, because this configuration is the more stable one. The accessible width for the case of the 5-site model is then

$$H' = H - 2z_0 + \sigma \tag{9}$$

where σ is the collision diameter of the hydrogen atom in Kollman's model. For the single wall, we find that $z_0 = 2.543$ Å for the Kollman model. This distance z_0, as in the case of the 1-site model, is a weak function of pore width. We list in Table 5 this value for 10 and 20 Å slit pores and for a single surface.

Pore Density. The pore density is, therefore, dependent on the choice of the volume. With the argument above on the accessible volume space for adsorbate molecules, we can define the average pore density as

$$\langle \rho \rangle = \frac{\langle N \rangle}{AH'} \tag{10}$$

where $\langle N \rangle$ is the ensemble average of the number of particles in the simulation box, A is the area of one graphite layer, and H' is the accessible pore width. The plot of $\langle \rho \rangle$ versus pressure is the adsorption isotherm at a given temperature.

The accessible pore width for the 1-site model is different from that for the 5-site model. Table 6 shows the accessible pore width for 10 and 20 Å physical width.

TABLE 5: Relationship between Zero-Potential Distance z_0 and Physical Width H for the 5-Site Model of Kollman et al

	z_0 (A)	
H (Å)	inverted pyramid	normal pyramid
10	2.2588	2.529
20	2.2794	2.542
∞	2.3086	2.543

TABLE 6: Accessible Pore Widths for 10 and 20 Å Slit Pores

physical pore width (Å)	accessible pore width (Å) for 1-site TRAPPE model	accessible pore width (Å) for 5-site Kollman model
10	7.7136	7.5694
20	17.675	17.564

Maximum Pore Density. Our choice of 10 Å in the above investigation was decided on the basis of the behavior of the maximum pore density versus pore width. The maximum pore density is defined as the pore density at the saturated vapor pressure. Figure 7 shows the maximum pore density for the 1-site model at 113 K.

The maximum pore density is based on the accessible width $H' = H - 2z_0 + \sigma^{(methane,methane)}$. We see that the maximum pore density exhibits a strong oscillation when the pore width is small, and this oscillation becomes less significant as the pore width becomes greater. We attribute the peaks to perfect pores, which are defined as pores that can pack an integral parallel number of layers, and the troughs are associated with imperfect pores whose widths are not large enough to pack an integral number of layers. From this plot, the perfect pores are 6.5, 10, and 12.5 Å, which are pores that can pack exactly one, two, and three layers, respectively. It is interesting to see the behavior of this maximum pore density versus pore width with respect to the saturated liquid density. When pore width is less than about 10 Å, the maximum pore density based on the accessible width $H' = H - 2z_0 + \sigma^{(methane,methane)}$ is less than the saturated liquid density. This simply reflects the imperfect packing of

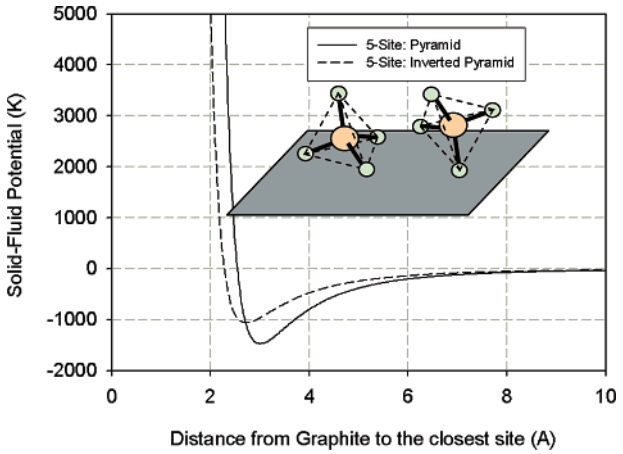

Figure 6. Solid−fluid potential of 5-site models for single surface (solid line, pyramid configuration; dashed line, inverted pyramid configuration).

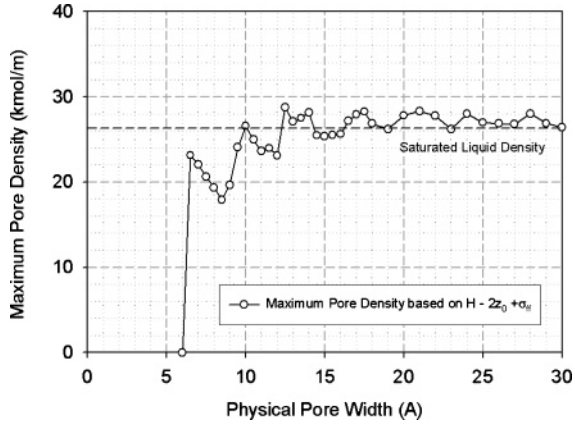

Figure 7. Maximum pore density of methane versus pore width at 113 K using the 1-site model.

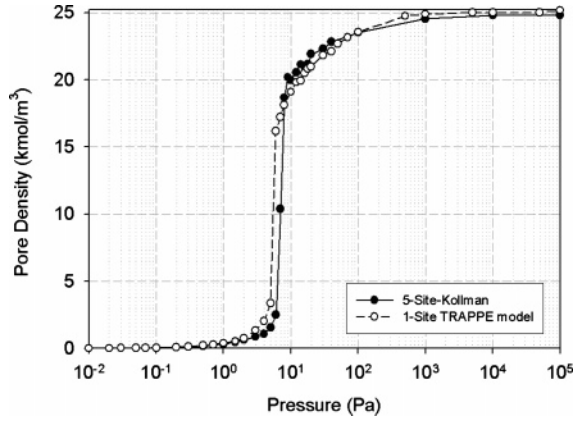

Figure 8. Adsorption isotherm of methane in a 10 Å slit pore at 113 K (dashed line, 1-site TRAPPE model; solid line, 5-site model).

molecules in small pores. When pore widths are greater than 20 Å, we see that the maximum pore density is slightly greater than the saturated liquid density, which is due to the combined effect of the dense first layers adjacent to the two pore walls and the better rearrangement of molecules in larger pores.

Slit Pore of 10 Å. Adsorption of methane in a 10 Å slit pore at 113 K is shown in Figure 8. The results from the 1-site model are shown as a dashed line with unfilled symbols, whereas those of the 5-site model are shown as a solid line with filled symbols.

These isotherms are reversible, and no hysteresis is observed. The isotherm exhibits the very sharp density change at about 6 Pa for the 1-site model, whereas the 5-site model has that sharp change at a slightly larger pressure of 8 Pa. This is due to the better packing of pseudo-spherical particles by the 1-site model in a confined space, and therefore the fluid−fluid interaction of this model is stronger in the confined space. Thus we see that in the confined space, the packing effect is important, and it is likely that the 1-site model over predicts the fluid−fluid interaction.

The transition in density at 6 or 8 Pa is due to the combination of the strong solid−fluid potential (which is the result of the overlap of two potentials exerted by the two walls in this 10 Å pore) and the fluid−fluid interaction, which arises from the interaction between molecules within the same layers adjacent to the surface but also between molecules of one layer and those of the other layer. Note that there are two layers that can be accommodated in this pore. The sharp change in the pore density at the transition pressure of 6 Pa (or 8 Pa in the case of 5-site model) does not reach the maximum density straight away, but rather the pore density reaches only about two-thirds of the maximum density. When the pressure is increased further from that transition pressure, the pore density increases gradually, a result of the compression of tightly packed molecules. The maximum pore densities of these models are less than the bulk saturated liquid density (26.3 kmol/m^3), which indicates that the state of the adsorbed phase as a whole is slightly less dense than the bulk liquid phase. The two models predict a somewhat comparable pore density. However, this could be misleading information about the packing efficiency in the 10 Å pore, because the accessible pore width of the 5-site model (7.5694 Å) is different from that of the 1-site model (7.7136 Å). To provide this information, we plot in Figure 9 the number of particles that resulted from the GCMC simulations using the 1- and 5-site models with the simulation box of the same size. We use the simulation box in which the linear dimensions in the *x* and *y* directions are 10 times the collision diameter. From

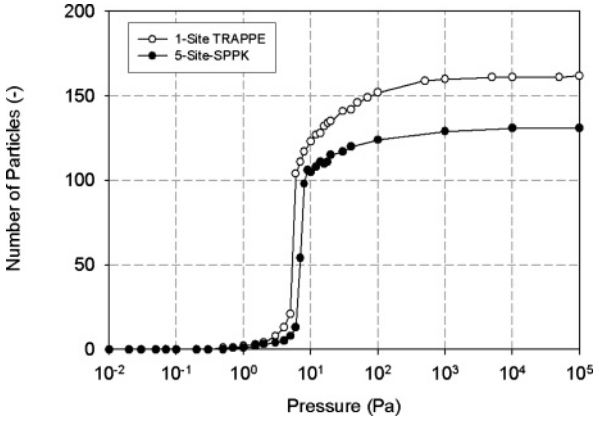

Figure 9. Number of particles versus pressure for a 10 Å slit pore at 113 K.

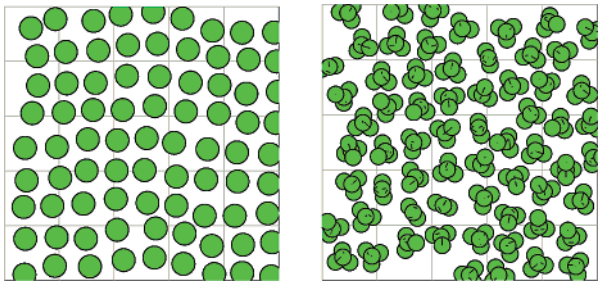

Figure 10. Snapshots of methane particles in a 10 Å pore at 113 K and 1000 Pa. Left, 1-site model; right, 5-site model (for clarity, the size of the particle is not to scale).

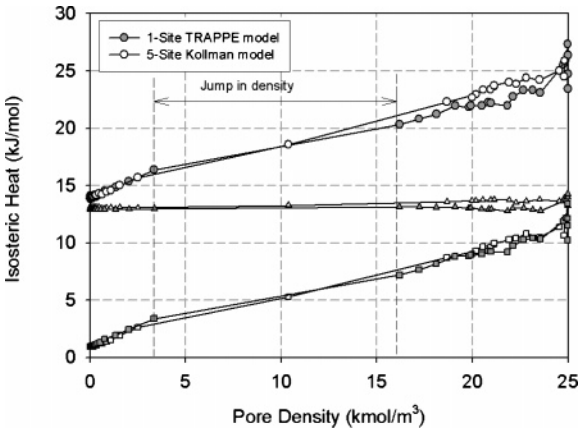

Figure 11. Isosteric heat of adsorption of methane in a 10 Å slit pore, contributed by solid−fluid interaction and fluid−fluid interaction (unfilled symbols, 5-site model; filled symbols, 1-site model).

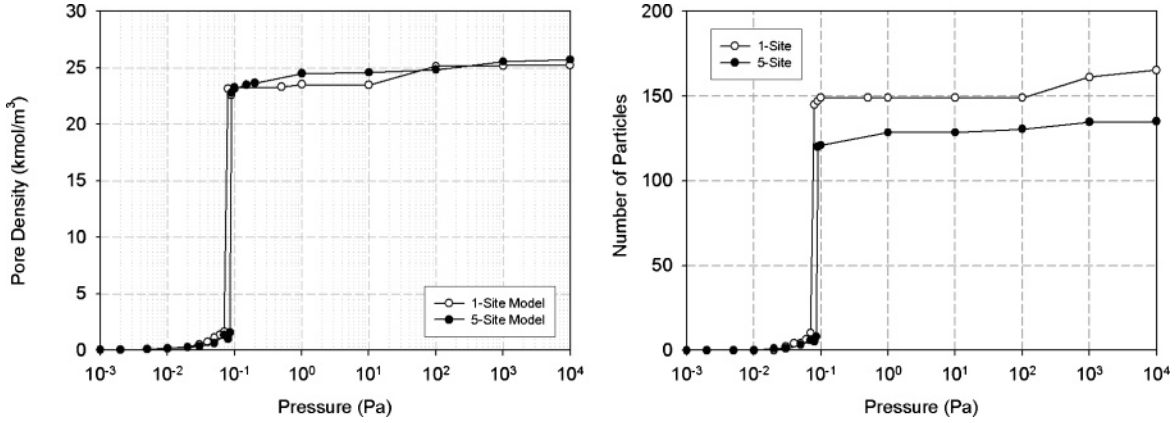

Figure 12. Adsorption isotherm of methane in a 10 Å slit pore at 90.7 K. Left, pore density (based on accessible pore width) versus pressure. Right, number of particles versus pressure.

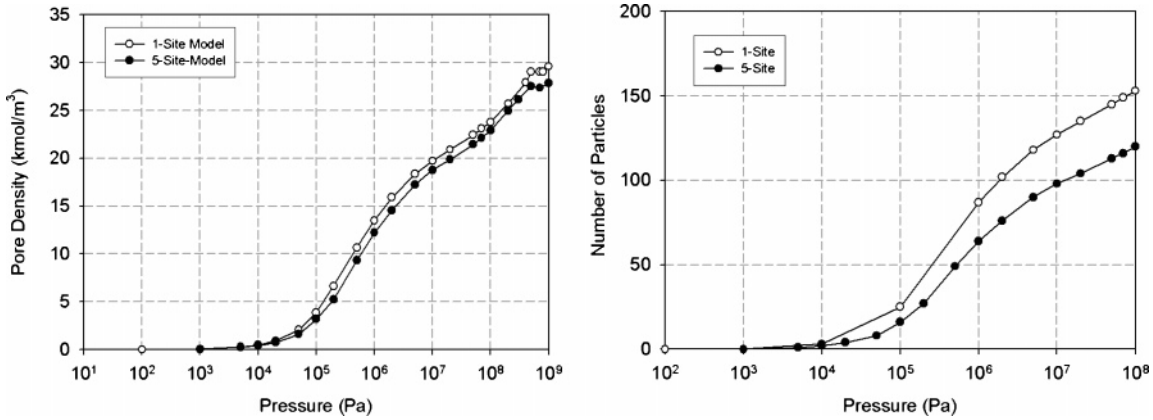

Figure 13. Adsorption isotherm of methane in a 10 Å slit pore at 273 K.

Figure 9, we see that with the same box size, the 1-site model predicts a greater number of particles that could be accommodated in the pore. Thus, this confirms that the packing is easier with the 1-site spherical particle. The difference between the 1- and 5-site models in the description of the adsorption isotherm for methane was also observed with the adsorption of methane in aluminophosphate[20,21] $AlPO_4$-5.

To further support the argument of better packing in a small pore by a spherical particle (1-site model), we show in Figure 10 the snapshots of methane particles in a 10 Å pore at 113 K and 1000 Pa. We clearly see that the 1-site model indeed produces a perfect hexagonal packing, whereas the 5-site model does not give packing as good as that of its 1-site counterpart.

Isosteric Heat. The GCMC simulation does not provide only the adsorption isotherm in pores but also the isosteric heat. Figure 11 shows the isosteric heat of methane adsorption in a 10 Å pore using the 1- and 5-site models.

This behavior of heat with respect to loading is typical for adsorption in pores. The isosteric heat contributed by the solid−fluid interaction is constant, and this constancy indicates that adsorption occurs at the two layers parallel and adjacent to the surface, that is, the centers of adsorbed molecules lie on a plane parallel to the carbon surface, and the position of this plane is at the minimum of the solid−fluid potential energy. The heat contributed by the fluid−fluid interaction shows a linear increase with loading, which is characteristic of fluid−fluid interaction, i.e., the greater the number of neighboring molecules the greater the heat associated with the fluid−fluid interaction. At the transition pressure in which the pore density jumps sharply, the isosteric heat contributed by the fluid−fluid interaction also exhibits a jump. This is simply because of the greater number of neighboring molecules to interact with after the jump has occurred.

10 Å Slit Pore of 10 Å at 90.7 K. To further test the packing effect in small pores, we consider two more temperatures. One is the lower temperature at the triple point, 90.7 K, and the other is the high temperature of the supercritical condition, 273 K. At lower temperatures, the intermolecular interaction is stronger, and as a result we would expect the stronger transition in density. This is indeed shown in the left plots of Figure 12.

Again we see the strong effect of packing in small pores, i.e., it is easier to pack molecules modeled as a spherical particle in the 1-site model compared to the packing of fused-five-sphere particles modeled in the 5-site model, as seen in the earlier onset of phase transition predicted by the 1-site model. After the transition, the 1-site model predicts a comparable pore density (based on accessible pore width) to the 5-site model. As in the previous case of 113 K, the comparable pore density based on accessible width does not convey information about the effectiveness of packing inside the pore. This information is provided in the right plots of Figure 12, where we plot the number of particles that can be packed inside the pore. The 1-site model predicts a greater number of particles that can be packed inside the pore. This again stresses the importance of the use of the correct potential model that accounts for the molecular structure in the calculation of pore density inside the confined space of slit pores.

Slit Pore of 10 Å at 273 K. Now we consider the supercritical conditions at 273 K. Figure 13 shows the adsorption isotherms of methane in 10 Å at this temperature over a very wide range of pressures. We see that the effect of packing in the confined space is very significant for supercritical conditions as well.

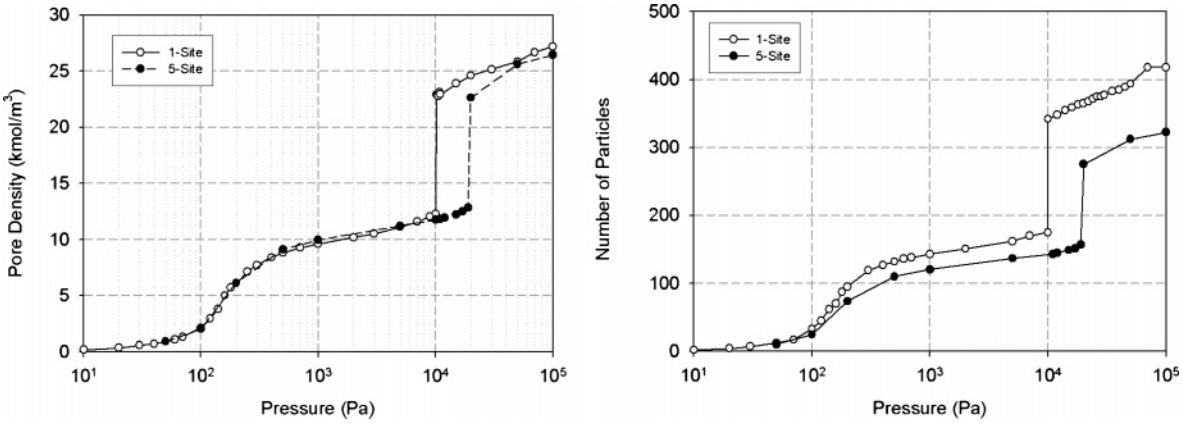

Figure 14. Adsorption isotherm of methane in a 20 Å slit pore at 113 K (solid line with unfilled symbols, 1-site model; dashed line with filled symbols, 5-site model).

The results for the 1-site model deviate from those of the 5-site model in the same way as we have seen earlier for subcritical conditions at 90.7 and 113 K. We thus argue that the 5-site model is very important for the correct description of methane in small pores in which the packing effect is important.

We note in Figure 13 that the 1-site model predicts a maximum pore density of 30 kmol/m^3 at a pressure of 1000 MPa, at which the bulk gas density is about 34 kmol/m^3. So the pore density at very high pressure is less than the bulk gas density because it is easier to orient molecules in the bulk phase than in the confined space of slit pores.

Slit Pore of 20 Å. Having discussed the behavior in a 10 Å pore at various temperatures, we turn to a larger pore, 20 Å. Figure 14 shows the adsorption isotherms using a box length of 10 times the collision diameter, and the cutoff radius is half of the box length. The GCMC simulation results for the 1-site model are plotted as a solid line with unfilled symbols, whereas those for the 5-site model are presented with half-filled symbols. The isotherm indicates an adsorption mechanism of molecular layering followed by pore filling. As in the case of 10 Å, we do not observe any hysteresis associated with the pore filling−emptying of this 20 Å pore.

Comparing the isotherms in terms of pore density (based on accessible pore width) between the two models, we see that they are comparable to each other during the molecular layering stage. This, however, becomes significant at the end of the molecular layering stage (prior to pore filling) and during the pore filling stage. As a result of the packing effect, the 5-site model predicts a higher pore-filling pressure (20 kPa compared to 10 kPa for the 1-site model), which is a result of the stronger fluid−fluid interaction as predicted by the 1-site model. Besides this evidence (phase-transition pressure) of better packing predicted by the 1-site model, we show in the right plots of Figure 14 the number of particles versus pressure. Again the behavior in larger pores is in agreement with what we have observed earlier with the smaller 10 Å pore.

4. Conclusions

We have presented in this paper the evaluation of the 1- and 5-site models for methane in terms of their performance in describing adsorption isotherm and isosteric heat. It is found that the 1-site model describes well for an open surface (comparable to that of the 5-site model), but in small pores it predicts a higher adsorption capacity (in terms of particle number) than the 5-site model, regardless of pore size, temperature, and pressure. This is attributed to the packing effect because the 1-site model treats the methane molecule as a spherical particle whereas the 5-site model describes it as a fused-five-sphere particle. Because of the simplistic spherical shape of the 1-site model, the packing is easier than what it should be, and therefore the capacity is over estimated. The extent of this over prediction is significant in small pores and when the pore is densely packed with molecules. It is argued that on the basis of the findings of this investigation, care should be exercised when simulation results from the 1-site model are used to describe adsorption in small pores.

Acknowledgment. This project is supported by the Australian Research Council.

References and Notes

(1) Avgul, N. N.; Kiselev, A. V. *Chemistry and Physics of Carbon;* Dekker: New York, **1970**. Vol. 6, p 1.
(2) Allen, M. P.; Tildesley, D. J. *Computer Simulation of Liquids*; Clarendon Press: Oxford, 1987.
(3) Frenkel, D.; Smit, B. *Understanding Molecular Simulations*; Academic Press: New York, 2002.
(4) El-Merraoui, M.; Aoshima, M.; Kaneko, K. *Langmuir* **2000**, *16*, 4300.
(5) Tanaka, H.; El-Merraoui, M.; Kodaira, T.; Kaneko, K. *Chem. Phys. Lett.* **2002**, *351*, 417.
(6) Murata, K.; Kaneko, K. *J. Phys. Chem. B* **2001**, *105*, 8498.
(7) Gardner, L.; Kruk, M.; Jaroniec, M. *J. Phys. Chem. B* **2001**, *105*, 12516.
(8) Kruk, M.; Li, Z.; Jaroniec, M.; Betz, W. *Langmuir* **1999**, *15*, 1435.
(9) Ryckaert, J.; McDonald, I.; Klein, M. *Mol. Phys*. **1989**, *102*, 2578.
(10) Moller, M.; Tildesley, D.; Kim, K.; Quirke, N. *J. Chem. Phys*. **1991**, *94*, 8390.
(11) Martin, M.; Siepmann, J. I. *J. Phys. Chem. B* **1998**, *102*, 2569.
(12) Sun, Y.; Spellmeyer, D.; Pearlman, D. A.; Kollman, P. *J. Am. Chem. Soc*. **1992**, *114*, 6798.
(13) Steele, W. A. *Surf. Sci*. **1973**, *36*, 317.
(14) Pascual, P.; Ungerer, P.; Tavitian, B.; Pernot, P.; Boutin, A. *Phys. Chem. Chem. Phys.* **2003**, *5*, 3684.
(15) Hill, T. *Statistical Mechanics*; Dover: New York, 1956.
(16) Munster, A. *Statistical Thermodynamics*; Springer: Berlin, 1969.
(17) Nicholson, D.; Parsonage, N. G. *Computer Simulation and the Statistical Mechanics of Adsorption*; Academic Press: London, 1982.
(18) Everett, D.; Powl, J. *J. Chem. Soc., Faraday Trans*. **1976**, *72*, 619.
(19) Kaneko, K.; Cracknell, R.; Nicholson, D. *Langmuir* **1994**, *10*, 4606.
(20) Boutin, A.; Pellenq, R. J. M.; Nicholson, D. *Chem. Phys. Lett.* **1994**, *219*, 484.
(21) Lachet, V.; Boutin, A.; Pellenq, R. J. M.; Nicholson, D.; Fuchs, A. H. *J. Phys. Chem*. **1996**, *100*, 9006.